Fungal Genetics and Biology 166 (2023) 103795

Contents lists available at ScienceDirect

Fungal Genetics and Biology

journal homepage: www.elsevier.com/locate/yfgbi

Proteomic dissection of the role of GliZ in gliotoxin biosynthesis in *Aspergillus fumigatus*

Aimee M. Traynor [a], Özlem Sarikaya-Bayram [a], Özgür Bayram [a], José Antonio Calera [b], Sean Doyle [a,*]

[a] Department of Biology, Maynooth University, Maynooth, Co. Kildare, Ireland
[b] Instituto de Biología Funcional y Genómica (IBFG-CSIC), Universidad de Salamanca, Salamanca, Spain; Departamento de Microbiología y Genética, Universidad de Salamanca, Salamanca, Spain

ARTICLE INFO

Keywords:
Quantitative proteomics
Fungal pathogen
Nutritional immunity
Transcription factor
Zinc
LC-MS
Mycotoxin

ABSTRACT

Gliotoxin (GT) biosynthesis in fungi is encoded by the *gli* biosynthetic gene cluster. While GT addition auto-induces biosynthesis, Zn^{2+} has been shown to attenuate cluster activity, and it was speculated that identification of Zn2Cys6 binuclear transcription factor GliZ binding partners might provide insight into this observation. Using the Tet-ON induction system, doxycycline (DOX) presence induced GliZ fusion protein expression in, and recovery of GT biosynthesis by, *A. fumigatus* Δ*gliZ*::HA-*gliZ* and Δ*gliZ*::TAP-*gliZ* strains, respectively. Quantitative RT-PCR confirmed that DOX induces *gli* cluster gene expression ($n = 5$) in both *A. fumigatus* HA-GliZ and TAP-GliZ strains. GT biosynthesis was evident in Czapek-Dox and in Sabouraud media, however tagged GliZ protein expression was more readily detected in Sabouraud media. Unexpectedly, Zn^{2+} was essential for GliZ fusion protein expression in vivo, following 3 h DOX induction. Moreover, HA-GliZ abundance was significantly higher in either DOX/GT or DOX/Zn^{2+}, compared to DOX-only. This suggests that while GT induction is still intact, Zn^{2+} inhibition of HA-GliZ production in vivo is lost. Co-immunoprecipitation revealed that GT oxidoreductase GliT associates with GliZ in the presence of GT, suggesting a potential protective role. Additional putative HA-GliZ interacting proteins included cystathionine gamma lyase, ribosomal protein L15 and serine hydroxymethyltransferase (SHMT). Total mycelial quantitative proteomic data revealed that GliT and GtmA, as well as several other *gli* cluster proteins, are increased in abundance or uniquely expressed with GT addition. Proteins involved in sulphur metabolism are also differentially expressed with GT or Zn^{2+} presence. Overall, we disclose that under DOX induction GliZ functionality is unexpectedly evident in zinc-replete media, subject to GT induction and that GliT appears to associate with GliZ, potentially to prevent dithiol gliotoxin (DTG)-mediated GliZ inactivation by zinc ejection.

1. Introduction

Gliotoxin (GT) biosynthesis is encoded by the *gli* cluster in the opportunistic fungal pathogen, *Aspergillus fumigatus*. It is now clear that Zn^{2+} availability and GT biosynthesis intersect on many levels: GT biosynthesis requires an essential Zn2Cys6 binuclear transcription factor, termed GliZ, for *gli* biosynthetic gene cluster expression (Bok et al., 2006), it is an auto-induced process (Cramer et al., 2006; O'Keeffe et al., 2014) and it is optimal under Zn^{2+}-limiting conditions (Saleh et al., 2018; Seo et al., 2019; Traynor et al., 2021; Vicentefranqueira et al., 2018). Indeed, at least one GT biosynthetic enzyme, a Cys-Gly carboxypeptidase GliJ, requires Zn^{2+} for activity (Marion et al., 2017), and GT *bis*-thiomethyltransferase activity is impeded by Zn^{2+} presence (Saleh et al., 2018). GT biosynthesis is also integrated into sulphur metabolism in *A. fumigatus* (Owens et al., 2015). Indeed, sulphur metabolism has been identified as a virulence factor with potential as a therapeutic target (Amich, 2022).

The zinc transcription factor ZafA enters the nucleus under zinc-limiting conditions (Vicentefranqueira et al., 2019), and drives GliZ-mediated *gli* expression and resultant GT biosynthesis (Traynor et al., 2021). It has also been shown that disruption of GT biosynthesis (*A. fumigatus* Δ*gliP*) led to overexpression of *zafA*, and resultant Zn^{2+} regulon genes (*zrfA*, *C* and *aspf2*), during infection of immunodeficient mice, compared to wild-type *A. fumigatus* (Liu et al., 2018). Fold-change

* Corresponding author.
E-mail address: sean.doyle@mu.ie (S. Doyle).

https://doi.org/10.1016/j.fgb.2023.103795
Received 17 November 2022; Received in revised form 30 March 2023; Accepted 31 March 2023
Available online 5 April 2023

A. fumigatus gene expression, by Nanostring analysis, during invasive growth in mouse lung compared to that during growth in **Aspergillus** minimal medium (AMM), revealed increased expression of *gli* genes (*gliG* (almost 10000-fold), *gliP* and *gliZ* (40-fold)) along with other up-regulated genes including *zrfC*, *zrfA*, *aspf2*, and *zafA*, which govern zinc uptake (Liu et al., 2021). These authors concluded that growth in the lung imposes limitation for key nutrients, including, but not only, Zn^{2+} on *A. fumigatus*. Overall, a hitherto cryptic link between GT biosynthesis and Zn^{2+} homeostasis is now apparent and dissection of GliZ functionality may reveal insight into this metallo-metabolite interaction.

GliZ is a Zn^{2+}-dependent DNA binding protein and dithiol gliotoxin (DTG), the reduced form of GT can both chelate free Zn^{2+} and also eject it from Zn^{2+}-metalloproteins of fungal (*A. fumigatus*) and animal (e.g., leukotriene A_4 hydrolase; LTA_4H) origin (König et al., 2019; Saleh et al., 2018). Moreover, Saleh et al. (Saleh et al., 2018) have elaborated that many previously identified GT inhibitory activities could, in fact have been instead due to DTG functionality. This raises the intriguing possibility that DTG chelation capacity could inhibit GliZ DNA binding activity, by Zn^{2+} ejection, and therefore attenuate GT biosynthesis unless GliT oxidises DTG to GT. Relevantly, GliZ has been characterised in the deep-sea-derived fungus *Dichotomomyces cejpii* and shown to bind to *gliG*, *gliM*, and *gliN* promoter regions in the *gli* cluster using electrophoretic mobility shift assay (Huang et al., 2019). Recent data suggest that intracellular and extracellular GT ratio is important for the control of GT production, however evidence of a sensing mechanism in *A. fumigatus* remains elusive. Since GliZ controls the expression of the GT biosynthetic genes, either GliZ or its interaction partners are strong candidates as components of such a regulatory circuit. The proteins interacting with GliZ and their regulatory roles are currently entirely unknown. More broadly, this occurrence of GT and related epipolythiodioxopiperazine (ETP) biosynthesis in many fungi (Ye et al., 2021a; Ye et al., 2021b; Ye et al., 2018), raises the possibility that Zn^{2+} may influence ETP biosynthesis in these species. Moreover, it is possible that ETPs, in general, may play a role in Zn^{2+} acquisition.

Despite a plethora of advances in the chemistry of GT biosynthesis and the regulation of *gli* cluster expression, and related ETP biosynthesis in many fungal species, the proteins interacting with GliZ and their regulatory roles are currently entirely unknown. Identification of any partners may improve our understanding as to how GT biosynthesis is integrated into fungal metabolism. Thus, the aim of this study was to make genetically-tagged GliZ, followed by confirmation and exploration of its expression in *A. fumigatus* by co-immunoprecipitation studies and quantitative proteomics to elucidate potential interaction partners.

2. Methods

Reconstitution of tagged-GliZ constructs in *Aspergillus fumigatus*

Table 1
Plasmids and strains used in this study.

Identifier Name	Design	Generation
Plasmids		
pCH008	Parent plasmid for pOFM16, 17 and 19	(Helmschrott et al., 2013)
pOFM16	*tetO-^{P}min::gliZ::3xha*	This study
pOFM17	*tetO-^{P}min:: 3xha::gliZ*	This study
pOFM19	*tetO-^{P}min:: tap::gliZ*	This study
Strains		
TDWC5.6	*ΔgliZ::pyrG; pyrG1*	(Bok et al., 2006)
AFPOFM16	*ptrA::tetO-^{P}min::gliZ::3xha; ΔgliZ::pyrG; pyrG1*	This study
AFPOFM17	*ptrA::tetO-^{P}min::3xha::gliZ; ΔgliZ::pyrG; pyrG1*	This study
AFPOFM19	*ptrA::tetO-^{P}min::tap::gliZ; ΔgliZ::pyrG; pyrG1*	This study

Δ*gliZ*. Primers and strains used for this study are shown in Table 1 and Supplementary Tables 1 and 2. *A. fumigatus* Δ*gliZ* (a kind gift from Professor N.P. Keller, U. Wisconsin-Madison) was transformed with 5′- and 3′- terminally TAP and 3 × HA-tagged *gliZ* open reading frames, initially under control of the endogenous promotor (unsuccessful, data not shown) and subsequently using the Tet-ON system using doxycycline (DOX) induction and selected based on pyrithiamine resistance. Following *A. fumigatus* Δ*gliZ* transformation and selection on pyrithiamine plates, Southern and Western blot analyses and RP-HPLC and LC-MS were used to assess successful target insertion and reconstitution of GT biosynthesis in *A. fumigatus* Δ*gliZ*. Endogenously expressed 3′ *gliZ::TAP* and *gliZ::HA* fusions could not be detected by Western blot analysis. In contrast, the 5′-tagged *TAP::gliZ* (pOFM19) and *HA::gliZ* (pOFM17) and the 3′-tagged, *gliZ::HA* (pOFM16) fusions expressed under Tet-ON promoter, which were readily detected by western-blot, were used for further studies.

pOFM16 was constructed as follows: *gliZ* ORF was amplified with oligos OFM52/56 and 3 × HA was amplified with OZG65/OFM57. These two fragments were fused to each other with OFM52/57 using fusion PCR, which was consequently cloned in a *PmeI/EcoR*V site of pCHOO8 plasmid (Helmschrott et al., 2013) (In-Fusion HD cloning kit, Clontech). For pOFM17, 3 × HA fragment was amplified with OFM58/59 and *gliZ* ORF with OFM60/55. These two fragments were fused to each other with fusion PCR (Yu et al., 2004; Nielsen et al., 2006) using OFM58/55 and cloned in *PmeI/EcoR*V site of pCHOO8 plasmid. For pOFM19, N-TAP fragment was amplified with OFM62/63 and *gliZ* ORF with OFM64/55. These two fragments were fused to each other with fusion PCR using OFM62/55 and cloned in PmeI/EcoRV site of pCHOO8 plasmid. Plasmids were sequenced in Eurofins sequencing facility (Germany, Eurofins).

Fungal culture and mycelial lysis. *A. fumigatus* wild-type (WT), Δ*gliZ*, and *HA-gliZ* strains (pOFM17) were maintained on Malt Extract agar (MEA) for 7 days at 37 °C. After incubation, conidia were harvested with PBST, washed three times with PBS and resuspended in PBS. Conidia were counted using hemocytometry and stored at 4 °C for future use. WT and Δ*gliZ* strains were grown in Sabouraud Dextrose (SAB) liquid for 24 h at 37 °C, shaking at 170 rpm. *HA-gliZ* cultures were grown in Potato Dextrose Broth (PDB) or SAB at 37 °C, shaking at 170 rpm for 21 h, followed by 3 h supplementation with DOX (60 μg/mL), and GT (5 μg/mL) or Zn^{2+} (25 μM). *HA-gliZ* cultures were grown in Czapek-Dox (CD) supplemented with Zn^{2+} (0, 1 or 25 μM) for 45 h followed by 3 h supplementation with DOX (60 μg/mL). Mycelia were then harvested and snap frozen in liquid N_2. Mycelial lysates were prepared in lysis buffer (100 mM Tris-HCl, 50 mM NaCl, 20 mM EDTA, 10 % (v/v) glycerol, 1 mM PMSF, 1 μg/ml pepstatin A, pH 7.5) with grinding, sonication and clarified using centrifugation. Lysate protein concentrations were assessed using a Qubit™ Protein Assay Kit (ThermoFisher Scientific). Protein lysates were snap frozen in liquid N_2 and stored at −20 °C until use.

Culture supernatant analysis by Agilent RP-HPLC and LC-MS. *A. fumigatus* culture supernatants from liquid cultures (SAB, 24 h + DOX, CD, 48 h + DOX) were centrifuged at 12,000*g* for 10 min. Aliquots were extracted in equal volume chloroform with vigorous shaking. Organic layers were isolated, dried by evaporation, and resuspended in 100 % methanol. This was followed by sonication for 3 min, and centrifugation at 13,000 × g for 10 min. Supernatants were analysed by RP-HPLC with UV detection (Agilent 1200 system), using a C8 RP-HPLC column (Agilent Zorbax Eclipse XDB-C8 Analytical; 5 μm particle size; 4.6 × 150 mm) at a flow rate of 1 mL/min. A mobile phase of water and acetonitrile with 0.1 % (v/v) trifluoroacetic acid, was used under various gradient conditions. All data were analysed using built-in GraphPad prism version 9.3.1 functions. For LC-MS detection of GT in culture supernatant, supernatant was analysed as previously described (Bayram et al., 2019; Mulvihill et al., 2017). Briefly, a nanoflow Agilent 1200 system for LC separation coupled to an Agilent 6340 Ion Trap for tandem MS was used. Samples were applied to a Zorbax SB-C18 HPLC-Chip with

a 40 nl trap column and a 75 μm × 43 μm (5 μm particle and 300 Å pore size) analytical column. GT (purity: 98 %) standards were obtained from Sigma-Aldrich.

RNA Extraction and RT-PCR. RNA extraction and RT-PCR was performed as described (Elramli et al., 2019). *A. fumigatus* strains were inoculated in triplicate in 50 mL of liquid SAB with (60 μg/mL) and without doxycycline at a concentration of 2×10^6 conidia/mL and incubated for 48 h on a shaker at 37 °C. Mycelia were filtered via miracloth and washed with diethylpyrocarbonate (DEPC) buffer (0.1 % DEPC in 1X PBS) three times. 100 mg of mycelia was collected and mRNA was extracted according to the RNeasy Plant Mini Kit protocol (Qiagen). mRNA was quantified according to the 'Qubit RNA BR Assay Kit' Protocol (Thermo Fisher). To synthesize complementary deoxyribonucleic acid (cDNA), 1 μg of mRNA was used for each strain and the 'Transcriptor First Strand cDNA Synthesis Kit' (Roche) was used. For qPCR experiments, cDNA of each duplicate strain was inoculated in triplicate in 96-well plates (Life Science Products). Plates were loaded in a LightCycler 480 qPCR machine (Roche). The cycle parameters were as follows: Pre-incubation (95 °C, 10 min), Amplification [40 cycles] (95 °C-10 s, 60 °C-20 s, 72 °C-10 s), Melting curve (65 °C to 97 °C with continuous fluorescence readings). Advanced relative quantification was used to determine the levels of gene expression in each strain. *actA* (actin) housekeeping gene was used as a reference. Relative expression analysis was performed by using the LightCycler 480 software. Bar charts represent the mean data of three combined biological replicates per strain, ± standard deviation.

SDS-PAGE and immunoblot analysis. Total protein concentrations of mycelial lysates were normalized prior to SDS-PAGE preparation. Lysate protein (60 μg) in reducing gel loading buffer was resolved using 12 % (w/v) SDS-PAGE and transferred onto nitrocellulose (NC) membrane using a Trans-Blot SD Semi-Dry transfer cell (Bio-Rad). After blocking (5 % (w/v) non-fat dry milk solution in PBST), membranes were probed for HA-GliZ presence using a monoclonal mouse IgG antibody against HA-tagged fusion proteins (GenScript). Primary antibody binding was detected using an anti-mouse IgG-horseradish peroxidase (HRP) conjugate (Bio-Rad). For chemiluminescent visualisation of all membranes, luminol as NUIMinol™ and H_2O_2 were added and membranes were exposed using the G:BOX Chemi XRQ (Syngene). Data was analysed using FIJI version 2.3.0 (Schindelin et al., 2012) for densitometry. Densitometry analysis was as follows: Developed blot images were set to greyscale and opened in FIJI. Protein band area was defined as a Region of Interest (ROI) using rectangle selection tool, adjusted to cover the whole area of the largest band in that row. The ROI was centred on each band of interest and a Mean Grey Value (MGV) measurement was taken using the Analyse > Measure tool. MGV was also recorded for background intensity of each lane on the blot. In Excel, MGV pixel density was inverted for each measurement through the following formula: 255 – X, where X is the measurement. Net MGV was calculated by subtracting the background MGV from the sample MGV of the same lane. Final relative quantity of protein bands were exported to GraphPad Prism version 9.3.1 for statistical analysis.

Co-Immunoprecipitation. *A. fumigatus* WT and HA-GliZ cultures were grown in SAB as described (to provide requisite mycelial mass). Mycelia were harvested and washed with ice-cold harvest buffer (1 % (v/v) DMSO, 100 μM PMSF in PBS) prior to snap-freezing. Mycelia were ground in liquid nitrogen and stored at −80 °C until use. Lysates were prepared in ice-cold protein extraction buffer (50 mM Tris-HCl, 150 mM NaCl, 10 % (v/v) glycerol, 0.1 % (v/v) NP-40 pH 7.5, supplemented with 1.5 mM DTT, 1X complete EDTA-free protease inhibitors (Roche), 1.5 mM benzamidine, 1 mM PMSF and 1X phosphatase inhibitors (1 mM NaF, 0.5 mM sodium orthovanadate, 8 mM β-glycerol phosphate) immediately prior to use. Resuspended mycelial lysates were centrifuged at 13,000*g* for 15 min at 4 °C. 1 mL of the protein supernatant was then collected into new Eppendorf tubes. For the immunoprecipitation of HA fusion proteins, anti-HA magnetic beads (Pierce) were washed twice with 20 volumes of protein extraction buffer containing supplements (as described above). The anti-HA beads were then resuspended in protein extraction buffer and added to crude protein extract. This mixture was left to incubate on a rotator at 4 °C for 3 h. Samples were placed in a magnetic rack to collect the beads and the supernatant was discarded. Beads were washed twice with protein extraction buffer (without supplements) and were then washed for a third time with the same buffer containing 1 mM DTT. All liquid was removed, and the beads were stored at −80 °C until further use (Frawley et al., 2020).

Co-IP LC-MS. Magnetic beads with bound protein were resuspended in extraction buffer (without supplements) by gentle pipetting. Non-reducing gel loading buffer was added and samples were boiled at 95 °C for 10 min. Beads were collected using a magnetic rack and protein samples were loaded onto 12 % (w/v) SDS-PAGE gels. Samples were run into gels to a depth of approx. 1 cm before visualisation by staining in Coomassie Blue and destaining in solvent solution (10 % glacial acetic acid, 30 % methanol). Proteins sections in each lane were sliced out of the gel and transferred into Eppendorf tubes. Gel pieces were subject to in-gel digestion with reduction-alkylation as per (Shevchenko et al., 2006). Samples underwent Zip-tip clean-up prior to LC-MS analysis. All peptide mixtures were analysed via a Thermo Fisher Q-Exactive mass spectrometer coupled to a Dionex RSLCnano. LC gradients ran from 3 to 50 % B over 35 min, and data was collected using a Top 15 method for MS/MS scans. LFQ proteomic analysis was performed using Proteome Discoverer (Version 1.4.0.288) alongside MaxQuant software (Version 2.1.0.0), with Andromeda used for database searching and Perseus (Version 2.0.3.0) used to organise the data.

HA-GliZ whole proteome analysis by LC-MS. Protein lysates from *A. fumigatus* Δ*gliZ*::*HA-gliZ* grown in SAB media for 21 h, with 3 h DOX induction only or in the presence of GT (5 μg/mL) or Zn^{2+} (25 μM), respectively, underwent dithiothreitol (DTT) reduction and iodoacetamide-mediated alkylation, followed by digestion using sequencing grade trypsin combined with ProteaseMax surfactant as previously described (Dolan et al., 2017). All peptide mixtures were analysed via a Thermo Fisher Q-Exactive mass spectrometer coupled to a Dionex RSLCnano. LC gradients ran from 4 to 35 % B over 2 h 15 min, and data was collected using a Top15 method for MS/MS scans. Comparative proteome abundance and data analysis was performed using MaxQuant software (Version 2.1.0.0), with Andromeda used for database searching and Perseus (Version 2.0.3.0) used to organise the data.

3. Results

DOX induces GT production by TAP-GliZ and HA-GliZ transformants. Tagged GliZ constructs were generated to allow exploration of GliZ expression, media-dependent abundance, ability to restore GT biosynthesis and interaction partners. The GliZ-tagged construct under the Tet-ON promoter is provided as Supplementary Fig. 1**.** Induction of tagged-GliZ expression in *A. fumigatus* Δ*gliZ*::HA-*gliZ* and Δ*gliZ*::TAP-*gliZ*, respectively, was observed by Western blot analysis following DOX induction **(**Fig. 1**a)**. While some degradation may have occurred in initial screening, intact HA-GliZ was detected in subsequent experiments. Parallel LC-MS analysis confirmed biosynthesis and secretion of GT from both transformant strains **(**Fig. 1**b)**. This indicated that tag presence did not completely interfere with GliZ functionality to enable *gli* cluster expression and GT biosynthesis in the transformants; nor did tag presence affect mycelial growth (+/- DOX induction) (Supplementary Fig. 2). In further optimisation experimentation, HA-GliZ was detectable in mycelial cell lysates after 24 h growth and DOX induction of *A. fumigatus* Δ*gliZ*::HA-*gliZ* **(**Fig. 1**c-e)**, and signal intensity was proportional to the amount of mycelial lysate subject to SDS-PAGE. No HA-GliZ was evident in the absence of DOX induction **(**Fig. 1**c-e)**. Quantitative RT-PCR experiments revealed that DOX induces the expression of several *gli* cluster genes other than *gliZ* in CD after 48 h. Genes *gliZ*, *gliT, gliP, gliA,* and *gliK* are increased with DOX addition to both Δ*gliZ*::HA-*gliZ* and Δ*gliZ*::TAP-*gliZ* transformants (Fig. 2).

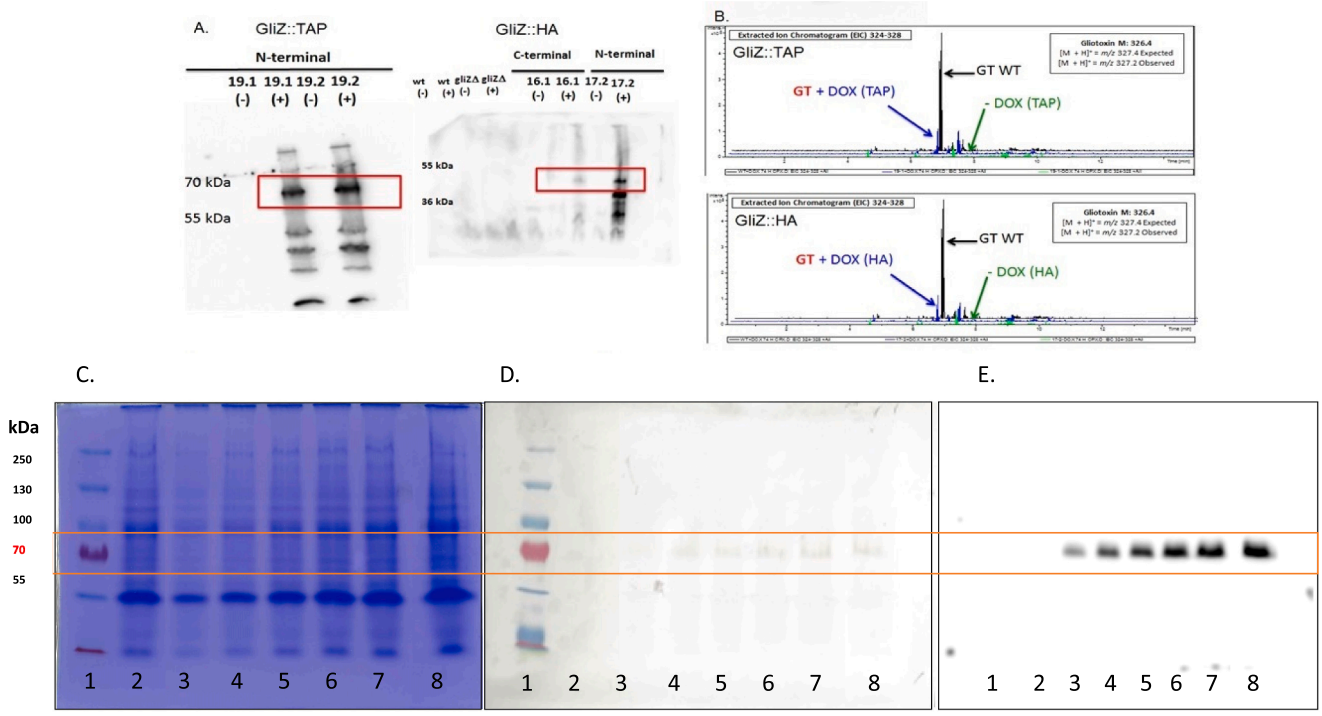

Fig. 1. GT secretion and GliZ immunodetection by strains carrying the TAP- and HA-GliZ tagged protein. A. Western blot confirmation of TAP-GliZ and HA-GliZ fusion protein expression under Tet-ON control in *A. fumigatus* strains grown in CD (DOX: doxycycline (+/-)). **B.** LC-MS analysis reveals that gliotoxin (GT) biosynthesis (blue) is evident only upon DOX addition to either *A. fumigatus* TAP-GliZ or HA-GliZ cultures. WT: GT production by *A. fumigatus* wild-type. HA-GliZ was used for subsequent Western blotting and Co-IP experimentation due to reagent availability. **C.** SDS-PAGE, **D.** Western blot stained in diamino benzidine (DAB), and **E.** Western blot stained with NUIMinol™ confirming the presence of HA-GliZ fusion protein in different total protein amounts of mycelial lysate (SAB media; 24 h DOX induction). Lane 1; MW ladder. Lane 2; -DOX lysate (54 μg protein loaded). Lane 3–8; +DOX lysate (15–54 μg total protein loaded per track).

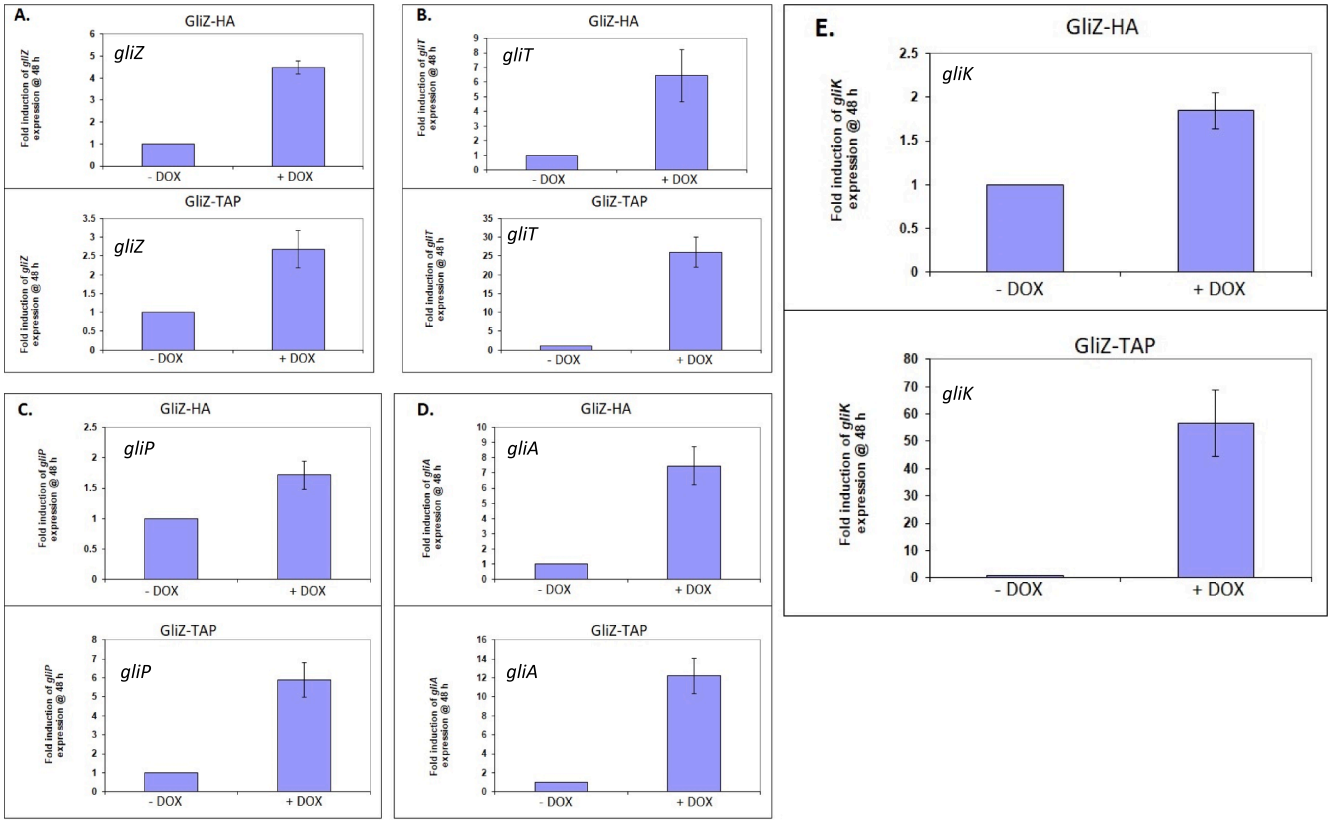

Fig. 2. Quantitative RT-PCR confirmation of *gli* cluster gene expression following DOX induction of tagged GliZ constructs compared to no DOX addition in fungus grown in CD. **A.** *gliZ* fold induction, **B.** *gliT* fold induction, **C.** *gliP* fold induction, **D.** *gliA* fold induction **E.** *gliK* fold induction.

GT and Zn^{2+} significantly augment DOX-induced HA-GliZ abundance in vivo. Analysis of HA-GliZ strain initially showed that DOX addition induced HA-GliZ expression over 24 h incubation (Fig. 1**c-e**). GT biosynthesis was also detected in culture media by RP-HPLC and LC-MS after 48 h DOX induction. GT biosynthesis was detected in both CD and SAB **(**Fig. 3**a).** Although GT biosynthesis was significantly higher in CD media and reduced by addition of Zn^{2+} (1 μM), SAB media also proved permissive for GT biosynthesis, conversely in a somewhat Zn^{2+}-independent manner **(**Fig. 3**a,b)**. RP-HPLC and LC-MS comparison to GT standard confirmed the identity of GT produced in SAB media (Fig. 3**b, c**). HA-GliZ production in CD after DOX induction for 3 h was found only with the addition of zinc (1 or 25 μM) to cultures possibly inferring some zinc requirement for GliZ function (Fig. 4**a,b**). Use of SAB facilitated generation of larger mycelial mass (Fig. 4**c**) and greater protein lysate concentration compatible with tagged-GliZ detection by immunoblot (Fig. 4**d**). DOX-induced HA-GliZ expression was evident at 24 h in SAB media following DOX addition at 21 h, suggesting 3 h was sufficient induction time to observe HA-GliZ presence **(**Fig. 5**a,b)**. Moreover, separate addition of either GT (5 μg/ml) or Zn (25 μM) for 3 h, in the presence of DOX significantly enhanced HA-GliZ abundance over the DOX exposure period as shown by Western blot analysis ($p < 0.05$; $p < 0.01$) **(**Fig. 5**a,b)**. To further resolve the relative importance of GT and Zn^{2+} presence during DOX induction of HA-GliZ in *A. fumigatus*, co-IP studies and LFQ proteomic analysis were undertaken.

Potential interaction partners of HA-GliZ. To ensure the most conservative interpretation of proteomic data, analysis of WT pull-down lysates identified 158 proteins which were assigned as non-specific binding proteins for the anti-HA paramagnetic beads (Supplementary Table 3). These proteins were removed from HA-GliZ pulldown datasets before further analysis. Replicate analysis of LFQ intensities of GliZ identified in co-IP pulldown samples showed no significant difference between Control (DOX only, no additions) or with GT or Zn^{2+} addition alongside DOX, respectively, which confirmed normalisation of protein quantity removed from solution by paramagnetic beads (Supplementary Fig. 3). Subsequently, three classes of proteins were identified including: **1.** Proteins identified as co-immunoprecipitated with HA-GliZ with known roles in GT biosynthesis or protein synthesis (Table 2). Including GliZ, 13 proteins were identified in this cohort. Eight proteins were

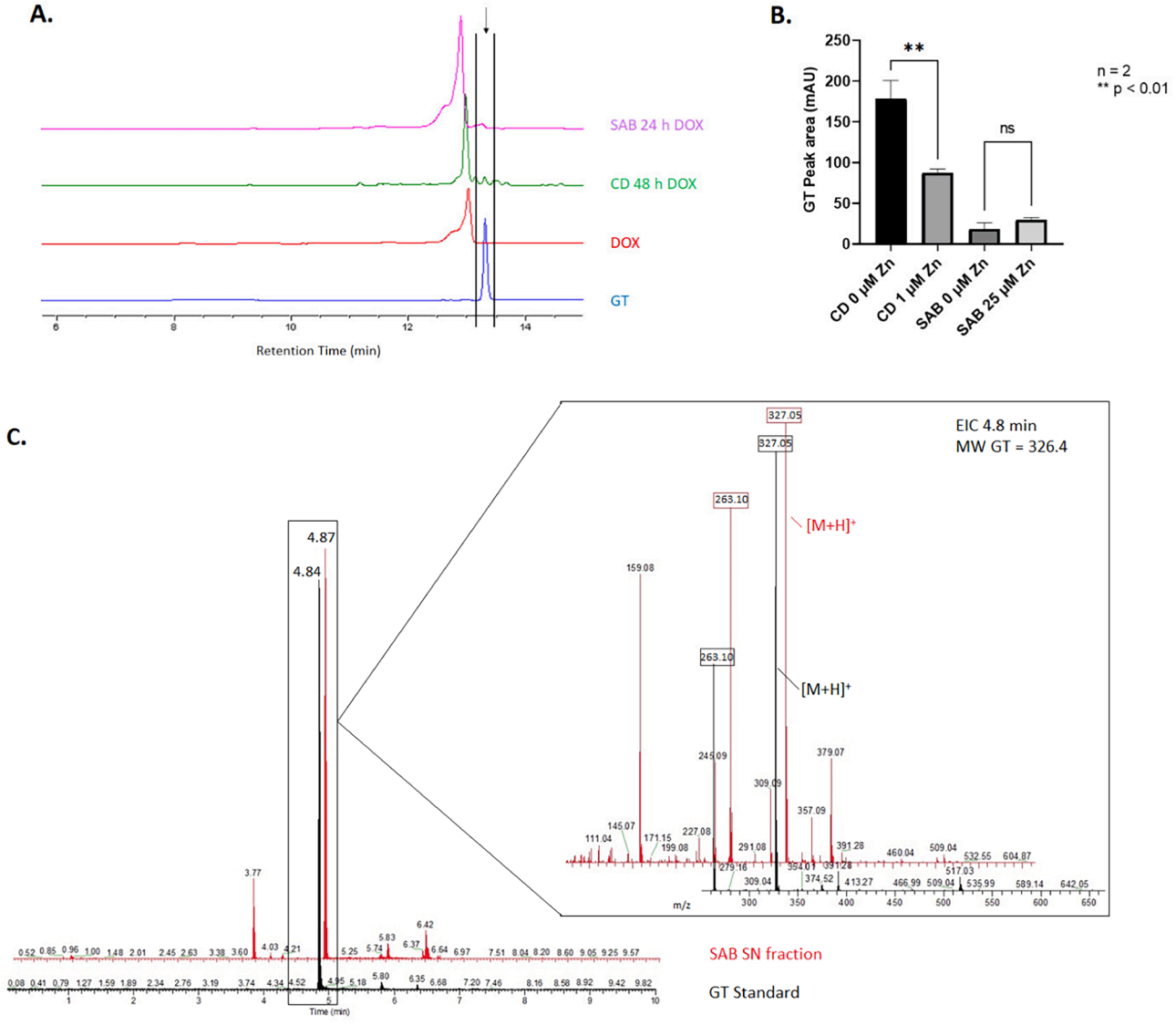

Fig. 3. Reconstitution of GT biosynthesis. HA-GliZ strain produces GT in liquid cultures when induced by DOX for 48 h in CD and 24 h in SAB. A. Representative chromatogram obtained from RP-HPLC data showing GT production in different culture media. **B.** GT peak areas obtained by RP-HPLC following differential culture reveal GT production in SAB in Zn^{2+}-independent. GT peak is indicated by arrow. CD: Czapek-Dox; SAB: Sabouraud Dextrose; DOX: Doxycycline standard; GT: Gliotoxin standard. **C.** Mass spectra in positive ion mode of culture supernatant confirming the identity of GT (M_r = 326.4) from isolated SAB supernatant (SN) compared to GT standard. 263.10 fragment ion is indicative of GT MS/MS.

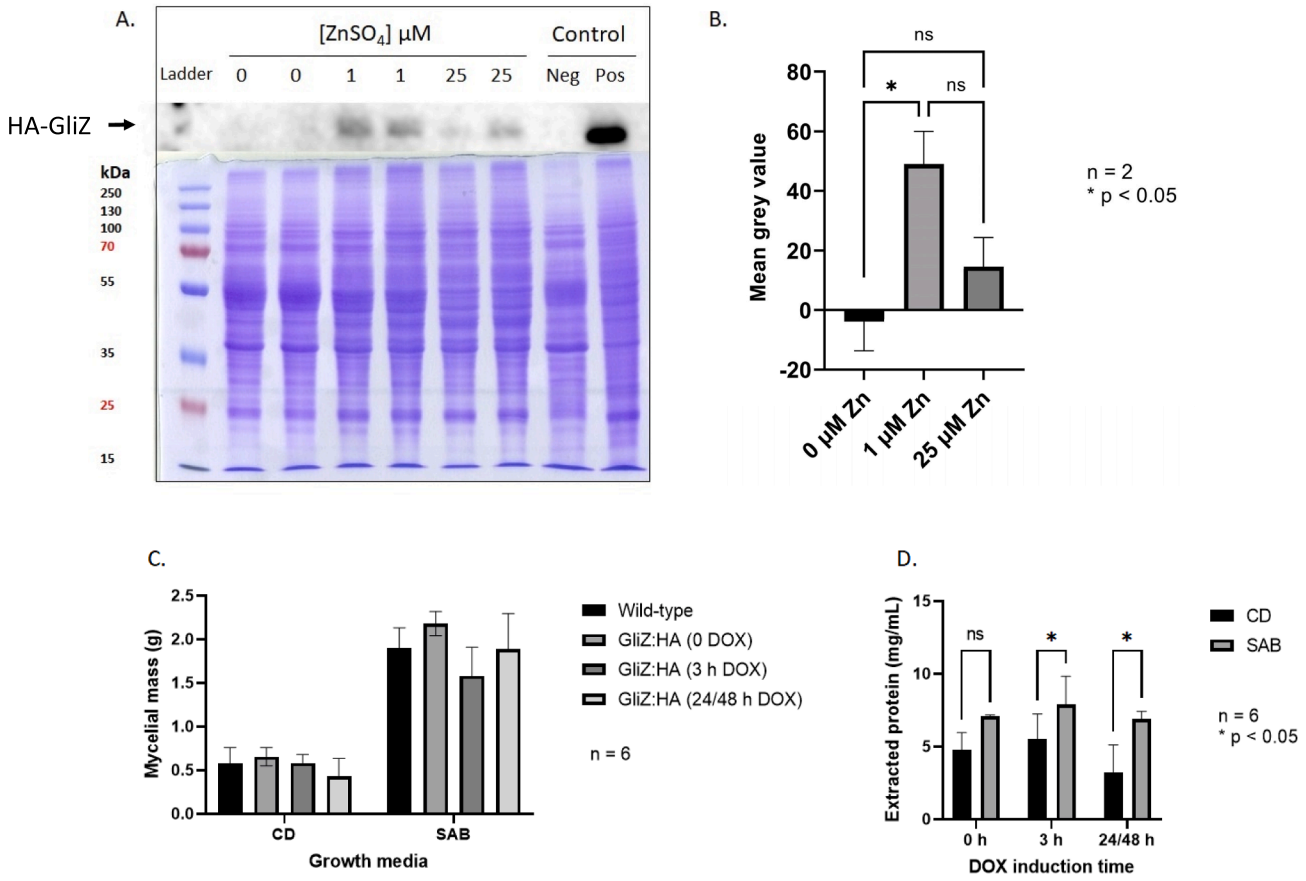

Fig. 4. Analysis of the HA-GliZ tagged protein after induction with DOX. A. Western blot and SDS-PAGE of fungal cultures in CD for 48 h and induced for 3 h with increasing zinc concentration and **B.** associated densitometry readings. Note: a densitometry value of < 0 indicates that the background reading was higher than the area of interest. Equal amounts of total protein were loaded per track. Positive and Negative controls are lysates from mycelia (+/- DOX induction). **C.** Comparison of mycelial weight (in grams) of *A. fumigatus* WT and Δ*gliZ*::HA-*gliZ* strains grown in either CD or SAB liquid broth for 48 and 24 h respectively. The timed addition of DOX (60 µg/mL) to tagged cultures is noted as either 0 h (no DOX addition), 3 h (added 3 h prior to harvest), or 24/48 h (added at inoculum). **D.** Comparison of protein concentrations obtained from HA-GliZ mycelial lysate grown in CD or SAB in the presence or absence of DOX.

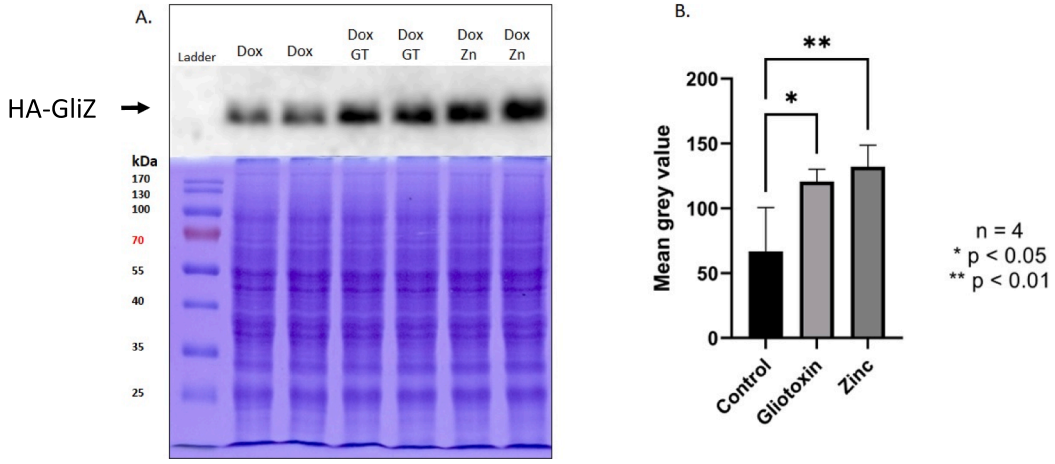

Fig. 5. HA-GliZ tagged protein is produced in the fungus cultured in SAB for 21 h before addition of DOX and after 3 h induction. **A.** Western blot and SDS-PAGE of SAB cultures post exposure to GT or Zn^{2+} in vivo for 3 h and **B.** associated densitometry readings.

identified in pulldowns from mycelial lysates, following GT exposure (3 h) during growth. Here, GT oxidoreductase GliT was uniquely present and was not detected in either control or Zn^{2+}-treated conditions (Table 2). Interestingly, 4 ribosomal proteins (ribosomal protein L1, 60S ribosomal protein L27a, 40S ribosomal protein S10b and ribosomal protein S13p/S18e) were uniquely identified in lysates pulldowns following Zn^{2+}-exposed growth conditions (Table 2). **2.** Six proteins were identified with potential roles in modulation of GT homeostasis or

Table 2
Proteins identified as co-Immunoprecipitated with HA-GliZ with known roles in GT biosynthesis or protein synthesis.

Protein Name	Control	Gliotoxin	Zinc	Protein IDs
C6 finger domain transcription factor **GliZ**	+	+	+	AFUA_6G09630
Eukaryotic translation initiation factor 3 subunit F	–	+	+	AFUA_1G09330
60S ribosomal protein L3 **Aspf 23**	–	+	+	AFUA_2G11850
60S ribosomal protein L23	–	+	+	AFUA_5G05630
Ribosomal protein L26	–	+	+	AFUA_6G11260
Eukaryotic translation initiation factor 3 subunit M	–	+	+	AFUA_7G03980
Translation elongation factor eEF-3, putative	–	+	+	AFUA_7G05660
Gliotoxin oxidoreductase **GliT**	–	+	–	AFUA_6G09740
Ribosomal protein L15	–	+	–	AFUA_1G04660
Ribosomal protein L1	–	–	+	AFUA_1G11710
60S ribosomal protein L27a, putative	–	–	+	AFUA_3G05600
40S ribosomal protein S10b	–	–	+	AFUA_6G12660
Ribosomal protein S13p/S18e	–	–	+	AFUA_6G13550

oxidoreductase activity and included serine hydroxymethyltransferase (SHMT) in all growth conditions, and cystathionine gamma-lyase (AFUA_8G04340) only in pulldowns from mycelial lysates following GT exposure (3 h) during growth (Table 3). **3.** Proteins with no known connection to GliZ or GT biosynthetic pathway. This cohort comprised 33 unique proteins, 5 of which were detected in all conditions, 9 only following GT or Zn^{2+} exposure during growth, 11 unique to GT presence and 8 detected only after only Zn^{2+}-exposure during mycelial culture (Table 4).

Quantitative proteomic changes following GT or Zn^{2+}-exposure. Whole cell lysates obtained from *A. fumigatus* Δ*gliZ*::HA-*gliZ* mycelia after 3 h exposure to GT or Zn^{2+} in the presence of DOX underwent LFQ LC-MS analysis. Two-sample t-tests were performed to identify proteins which were significantly altered in abundance between conditions, with a p-value of < 0.05 and a Log_2 difference value $> \pm 1$ as the cut-off. Four proteins were significantly altered in abundance in GT-treated mycelia compared to control, one protein was significantly decreased in abundance in Zn^{2+} compared to control, and the abundance of nine proteins was significantly different between GT and Zn^{2+}-treated samples (Table 5). Serine hydroxymethyltransferase SHMT (termed Shm2 in (Bacher et al., 2014)) was identified as decreased in abundance with GT addition. This enzyme is involved in the interconversion of tetrahydrofolate and the production of L-serine from glycine. GliT, the enzyme responsible for oxidation of intracellular DTG to GT prior to efflux, was increased in abundance after 3 h growth in the presence of exogenous GT. Also increased in abundance was the GT thiomethyltransferase GtmA (termed TmtA in (Scharf et al., 2014)) which converts DTG into bisdethio bis(methylthio)gliotoxin (BmGT) using *S*-adenosylmethionine (SAM) as a methyl source. A glutathione synthetase (GSH-S) was found

Table 3
Proteins identified by HA-GliZ co-IP with potential roles in modulation of GT homeostasis or oxidoreductase activity.

Protein Name	Control	Gliotoxin	Zinc	Protein IDs
Serine hydroxymethyltransferase **SHMT**	+	+	+	AFUA_3G09320
Squalene epoxidase **Erg1**	–	+	+	AFUA_5G07780
Choline oxidase, putative **CodA**	–	+	–	AFUA_8G04090
Putative cystathionine gamma-lyase	–	+	–	AFUA_8G04340
Ortholog(s) have cytochrome-c oxidase activity	–	+	–	AFUA_Mt00120
Nitrite reductase **NiiA**	–	–	+	AFUA_1G12840

Table 4
Proteins identified by co-IP with unknown connection to GliZ or GT biosynthetic pathway.

Protein Name	Control	Gliotoxin	Zinc	Protein IDs
Endoplasmic reticulum chaperone **BipA**	+	+	+	AFUA_2G04620
Secretion related GTPase **SrgB/Ypt1**	+	+	+	AFUA_5G04320
Triosephosphate isomerase	+	+	+	AFUA_5G13450
Nascent polypeptide-associated complex subunit alpha **Egd2**	+	+	+	AFUA_6G03820
Tubulin beta chain	+	+	+	AFUA_7G00250
Polyadenylate-binding protein **Pab1**	–	+	+	AFUA_1G04190
Non-specific serine/threonine protein kinase	–	+	+	AFUA_1G11080
Inosine-5′-monophosphate dehydrogenase	–	+	+	AFUA_2G03610
Dipeptidyl-peptidase 5 **DppV**	–	+	+	AFUA_2G09030
Nucleolar protein	–	+	+	AFUA_3G09600
Nucleolar protein 58 **Nop58**	–	+	+	AFUA_3G13400
Histone 2A.Z	–	+	+	AFUA_5G10950
Nucleoside diphosphate kinase **Ndk1**	–	+	+	AFUA_5G03490
Uncharacterised protein	–	+	+	AFUA_6G02870
Prohibitin	–	+	–	AFUA_1G13470
Argininosuccinate synthase	–	+	–	AFUA_2G04310
Calcium/calmodulin-dependent protein kinase, putative	–	+	–	AFUA_2G13680
T-complex protein 1 subunit alpha	–	+	–	AFUA_2G16020
Phosphoglucomutase **PgmA**	–	+	–	AFUA_3G11830
ATP-dependent RNA helicase **Ded1**	–	+	–	AFUA_4G07660
Nitrilase	–	+	–	AFUA_6G13450
Clathrin heavy chain	–	+	–	AFUA_4G07700
Oxoglutarate dehydrogenase (succinyl-transferring)	–	+	–	AFUA_4G11650
Septin	–	+	–	AFUA_5G03080
FK506-binding protein 4	–	+	–	AFUA_6G08580
Uncharacterised protein	–	–	+	AFUA_1G02710
Fasciclin domain family protein	–	–	+	AFUA_1G14300
Branched-chain-amino-acid aminotransferase	–	–	+	AFUA_2G10420
RNP domain protein	–	–	+	AFUA_5G07120
Dynamin GTPase, putative	–	–	+	AFUA_6G11890
Secreted beta-glucosidase **Sun1**	–	–	+	AFUA_7G05450
Alanine–tRNA ligase	–	–	+	AFUA_8G03880
Probable beta-glucosidase **BtgE**	–	–	+	AFUA_8G05610

to be increased in abundance in GT treated, compared to Zn^{2+} treated, samples. Elevated amounts of a dual functional catalase-peroxidase Cat2 were observed with GT addition compared to the control or Zn^{2+}-treated samples. This suggests an increase in oxidative stress or redox cycling in the cell during exogenous GT presence. Only one protein was found to have significantly altered abundance under Zn^{2+} addition compared to control, the Homogentisate 1,2-dioxygenase HmgA. This protein plays a role in the L-tyrosine degradation pathway and is involved in the production of a second form of melanin, pyomelanin (Schmaler-Ripcke et al., 2009)

Many proteins were identified as uniquely detected under certain conditions. Likewise, some proteins were found to be absent under one condition but detected in both other sample groups. Analysis of GT-treated samples found 23 proteins which were unique to GT addition, and 14 proteins which were absent (Table 6). Among the uniquely identified proteins were three proteins from the *gli* cluster, GliM, GliN and GliG. Of note is the unique presence of a novel methyltransferase MtrA (AFUA_6G12780), shown to be important for GT self-defence in

Table 5
Proteins identified as significantly ($p < 0.05$) altered in abundance after induction for 3 h with DOX in the presence of GT or Zn.

Protein Name	Log_2 Fold Change	p-value	Peptides	Sequence [%]	Protein IDs
GT versus Control					
Serine hydroxymethyltransferase **SHMT**	−1.15735	0.0177139	34	66.7	AFUA_3G09320
Catalase-peroxidase **Cat2**	1.61899	0.002333	31	53.9	AFUA_8G01670
Gliotoxin thiomethyltransferase **GtmA**	3.49748	1.95E-05	11	47.4	AFUA_2G11120
Gliotoxin oxidoreductase **GliT**	4.04698	0.000116	22	84.4	AFUA_6G09740
Zn versus Control					
Homogentisate 1,2-dioxygenase **HmgA**	−1.10004	0.00419	14	56.3	AFUA_2G04220
GT versus Zn					
Serine hydroxymethyltransferase **SHMT**	−1.23097	0.019186	34	66.7	AFUA_3G09320
Phosphoketolase	−1.13604	0.008053	14	23.4	AFUA_3G00370
Enoyl-CoA hydratase/isomerase family protein	−1.00944	0.046748	7	34.7	AFUA_2G10920
Uncharacterized protein	1.0076	0.026115	4	23.9	AFUA_4G07030
1-aminocyclopropane-1-carboxylate deaminase	1.15286	0.024694	5	26.6	AFUA_2G01030
Glutathione synthetase, **GSH-S**	1.2225	0.023128	8	29.5	AFUA_5G06610
Catalase-peroxidase **Cat2**	1.61481	0.000656	31	53.9	AFUA_8G01670
Gliotoxin thiomethyltransferase **GtmA**	3.46776	0.001247	11	47.4	AFUA_2G11120
Gliotoxin oxidoreductase **GliT**	4.77642	0.001151	22	84.4	AFUA_6G09740

Aspergilli, particularly the GT producer *A. fumigatus* and the non-producing species *A. nidulans* (de Castro et al., 2022). Importantly, an assimilatory sulfite reductase (AFUA_6G08920) was identified, which is involved in the reduction of sulfite to sulfide, that is in turn used to produce L-cysteine (Amich et al., 2016; Amich et al., 2013). Several ribosomal proteins including ribosomal protein L15, and the serine/threonine protein phosphatase CnaA were also identified. SidA, the L-ornithine N(5)-monooxygenase responsible for the first step in production of *A. fumigatus* hydroxymate siderophores, was also uniquely detected in GT addition (Table 5). Of the proteins which were found to be absent after GT exposure, of interest are a Zn^{2+}-binding alcohol dehydrogenase and another member of the serine/threonine protein phosphatase family. Also identified as uniquely absent are two proteins with domains of unknown function (DUF proteins). DUF636 (AFUA_3G01340) has domains which are involved in carbon–sulphur lyase activity and Zn^{2+}-binding domains. DUF4440 (AFUA_2G00790) has similarity with nuclear transport factor (NTF2) domain proteins.

Notably, 52 proteins were uniquely detected in HA-GliZ cultures when induced with DOX and Zn^{2+} for 3 h, while 6 proteins were subsequently found to be absent in these samples (Supplementary Table 4). The CCAAT-binding factor complex subunit HapC was uniquely present under these conditions. In eukaryotes this protein is responsible for redox status sensing of cells via protein thiol group oxidation (Thon et al., 2010). Another protein which was uniquely found after Zn^{2+}-supplementation is a non-ribosomal peptide synthetase (NRPS) termed Pes1 which is essential to produce the secondary metabolite fumigaclavine C (O'Hanlon et al., 2012). Several proteins which make up the vesicle cellular component are also found to be uniquely detected. Included among the proteins absent in samples after Zn^{2+}-addition were a putative 1,3-beta-glucan biosynthesis protein, and a sulfhydryl oxidase.

Gene ontology analysis using online tool g:Profiler (version e106_eg53_p16_65fcd97) was used to investigate the molecular functions (MF), biological processes (BP), and KEGG pathways which were enriched in certain groups of identified proteins (Raudvere et al., 2019). There were several observations of particular interest (Supplementary Table 5). In the subset of proteins uniquely present in the presence of GT, several proteins with methyltransferase activity or involved in the structural constituent of the ribosome were observed. Opposing this was the observation that proteins with metal ion binding functionality were found to be uniquely absent after GT addition. When Zn^{2+} was added during the culture of *A. fumigatus* Δ*gliZ*::HA-*gliZ*, proteins involved in vesicle mediated transport and the phagosome were uniquely detected (Supplementary Table 5).

Whole cell lysate (WCL) proteomics and co-IP datasets were further analysed to identify proteins which were uniquely identified or significantly altered in abundance in the whole cell that associate with and are potential GliZ interaction partners. Six proteins were identified in both datasets (Supplementary Table 6). GliT was uniquely found to associate with GliZ in the presence of GT, while it is increased in abundance with GT addition in whole cell proteomics. Ribosomal protein L15 was identified as uniquely associated with 3 h GT incubation in both analyses. SHMT was identified as co-precipitating with GliZ under all conditions but was found to be decreased in abundance with the addition of GT for 3 h in WCL. A stomatin family protein was found to be potentially complexed in all conditions of the co-IP analyses but was seen to be uniquely present in Zn^{2+} -treated WCL samples. Two other proteins are also found in both datasets – ATP-dependant RNA helicase Ded1, and 40S ribosomal protein S10b – however they were identified in different conditions in the co-IP and WCL proteomics.

4. Discussion

Here we reveal that DOX-induced expression of HA-GliZ is detectable, and results in GT biosynthesis and secretion from *A. fumigatus*. Although the expressing strain is less sensitive to Zn^{2+} regulation, the *gli* BGC still retains a GT-mediated regulation phenotype, along with a requirement for Zn^{2+} presence - the latter possibly due to its role in conferring GliZ stability. We also identify potential GliZ binding partners, particularly GliT, which suggests a role for this oxidoreductase in protecting GliZ integrity by ensuring that essential Zn^{2+} cannot be removed by the potent chelator, DTG. In addition, we uncover evidence of new elements of integrated sulphur/Zn^{2+}/GT metabolism using LFQ proteomic analysis. This work has the potential to enhance our understanding of the paradoxical requirement of Zn^{2+} to enable GliZ activity, yet the multiple independent observations that GT biosynthesis can be inhibited by Zn^{2+} presence. Hence, it addresses the growing area of metallo-metabolite interactions in fungi.

Zn^{2+} regulates expression of the *gli* BGC, is also directly required for GliZ activity as a Zn2Cys6 binuclear transcription factor (Bok et al., 2006; Forseth et al., 2011; Vicentefranqueira et al., 2018) and we sought to dissect same via construction of GliZ-tagged *A. fumigatus*. Unfortunately, reconstitution of tagged *gliZ* constructs, into *A. fumigatus* Δ*gliZ*, under the control of its native promoter did not result in either detectable *gliZ* gene expression, the presence of affinity tagged GliZ protein or GT biosynthesis. We speculate that this could be due to the transient expression of low levels of GliZ and the use of culture conditions optimal for GT biosynthesis (CD media), as opposed to biomass production. Additionally, GliZ instability due to structural alterations cannot be ruled out.

Fortunately, deployment of Tet-ON system facilitated *gliZ* expression and tagged GliZ protein production resulted in detectable GT

Table 6
Identified proteins which are uniquely present or absent in HA-GliZ mycelia induced with DOX and treated with GT for 3 h.

Protein Name	Peptides	Sequence [%]	Protein IDs
Uniquely identified in the presence of GT			
O-methyltransferase **GliM**	9	28.8	AFUA_6G09680
Ribosomal protein L15	6	27.2	AFUA_1G04660
N-methyltransferase **GliN**	4	32.6	AFUA_6G09720
Glutathione S-transferase **GliG**	6	24.6	AFUA_6G09690
40S ribosomal protein S10b	4	26.5	AFUA_6G12660
Methyltransferase **MtrA**	8	33.6	AFUA_6G12780
Heat shock protein Hsp30-like, putative	4	54.9	AFUA_6G06470
Methyltransferase, putative	4	13.8	AFUA_3G13140
SNARE domain protein	3	18.3	AFUA_7G01510
40S ribosomal protein S25	4	26.9	AFUA_1G16523
Assimilatory sulfite reductase	8	12.3	AFUA_6G08920
4-nitrophenylphosphatase, PNPPase	3	13.6	AFUA_3G08310
Checkpoint protein kinase **SldA**, putative	3	7.1	AFUA_6G08120
Mitochondrial ribosomal protein *L*11, putative	3	33.3	AFUA_5G11830
Uncharacterized protein	3	17.9	AFUA_6G09745
Protein transport protein **Sec13**	3	16.7	AFUA_4G06090
Transcription elongation factor **Spt5**	6	11.1	AFUA_4G08500
Serine/threonine-protein phosphatase 2B catalytic subunit, **CnaA**	6	19.7	AFUA_5G09360
GTPase activating protein **Gyp5**, putative	2	4.4	AFUA_4G10600
Uncharacterized protein	3	8.2	AFUA_6G09390
L-ornithine N(5)-monooxygenase **SidA**	3	8.6	AFUA_2G07680
Phosducin, putative	2	8.9	AFUA_5G12200
NUDIX domain protein	2	10	AFUA_6G11490
Uniquely absent in GT addition			
Zinc-binding alcohol dehydrogenase, putative	3	13	AFUA_8G02430
Ser/Thr protein phosphatase family	4	12.9	AFUA_3G04160
DUF636 domain protein	7	67.1	AFUA_3G01340
DUF4440 domain-containing protein	3	33.6	AFUA_2G00790
Cytidine deaminase, putative	4	43	AFUA_7G01040
Carnitine acetyl transferase	4	8.5	AFUA_1G12340
UBX domain protein **Ubx5**, putative	2	6.3	AFUA_7G04320
DNA-directed RNA polymerase subunit	3	47.7	AFUA_2G08540
Arsenate reductase **ArsC**, putative	3	53.3	AFUA_1G16090
Pre-rRNA processing protein **Tsr1**, putative	5	11	AFUA_2G12880
Hydroxyacid-oxoacid transhydrogenase	5	18.4	AFUA_2G04520
Mitochondrial import inner membrane translocase subunit **Tim9**	4	56.7	AFUA_2G01050
Uncharacterized protein	4	45.8	AFUA_1G00760
NAD(+) diphosphatase	3	11.2	AFUA_5G03360

biosynthesis, in CD, PDB and SAB media, following DOX addition. This is in accordance with reconstitution of *gliZ* expression in *A. fumigatus* Δ*gliZ*, and consequent GT biosynthesis, although we did not detect altered production of other metabolites, as previously noted (Bok et al., 2006). Interestingly, DOX addition for 3 h in SAB media, with either GT or Zn^{2+} co-addition resulted in increased HA-GliZ detection by Western analysis compared to DOX-only presence. This aligns with GT-induced *gliZ* expression but is somewhat at variance with the observed down-regulation of GT biosynthesis by Zn^{2+} (Saleh et al., 2018; Schrettl et al., 2010; Seo et al., 2019; Traynor et al., 2021). We speculate that it is possible that deployment of the Tet-ON system has partially or completely dysregulated Zn^{2+}-influenced *gli* cluster expression, but not affected the Zn^{2+} requirement for GliZ activity as a Zn2Cys6 binuclear transcription factor. In CD media, which is generally permissive for GT biosynthesis, Zn^{2+} addition is a requirement to produce the tagged GliZ protein. In the absence of Zn^{2+}, no HA-GliZ signal is detected. However, the addition of 1 or 25 μM zinc to cultures is permissive for tagged protein production. Thus, we speculate that Zn^{2+} may enhance GliZ stability in vivo in our engineered strain where the Tet-ON system drives *gli* cluster expression in a Zn^{2+}-independent manner. However, it could also be possible that the Tet-ON promoter might not function properly under zinc-limiting conditions.

After co-immunoprecipitation of HA-GliZ from different stringently-controlled conditions, we found that GliT interacts with GliZ in the presence of GT. It is known that DTG is capable of binding Zn^{2+} and ejecting it from metalloproteins (Saleh et al., 2018). The association with GliZ suggests that GliT could act in a localised protective manner by preventing DTG-mediated inactivation of the zinc-finger regions on the GliZ transcription factor. This complements pre-existing data wherein GliT has been shown to have self-protective effects in *A. fumigatus* against endogenous GT toxicity, as well as conferring protection against GT to non-producing species (Schrettl et al., 2010; Scharf et al., 2010) through the prevention of intracellular glutathione depletion. We observed eight ribosomal proteins and two subunits of eukaryotic translation initiation factor (eIF-3) co-precipitating with GliZ under varying spiked conditions (Table 2). Of particular interest is ribosomal protein L15, which is uniquely found in the presence of GT in both co-IP and WCL datasets. Whether this observation suggests a link between *gli* cluster expression and translation, or results from GT-induced ribosomal precipitation remains to be elucidated. Another associated protein is serine hydroxymethyltransferase (SHMT) which was identified in all conditions (Table 3). This protein is involved in one-carbon metabolism and the interconversion of serine and glycine using tetrahydrofolate. This is of interest as it is also observed to be decreased in abundance in response to GT in WCL proteomics (Supplementary Table 6) and SHMT is noted to have Zn^{2+}-binding functionality and human immunogenic properties (Singh et al., 2010; Bacher et al., 2014). The connection between inducing GT biosynthesis via GliZ and sulphur metabolism is further supported by the identification of cystathionine gamma lyase in GT treated samples (Table 3). This protein is integral to the *A. fumigatus* sulphur metabolism pathway, converting cysteine to cystathionine, which feeds into the methyl-methionine cycle to produce SAM, as well as being connected to the GSH metabolic pathway (de Castro et al., 2022; Traynor et al., 2019). Sulphur metabolism is not only important for GT biosynthesis, but also to produce the sulphur metabolite ergothioneine (EGT) (Sheridan et al., 2016; Traynor et al., 2019). Many proteins with an unknown relationship to GT biosynthesis (Gomez-Lopez et al., 2022) or metal homeostasis are found to be co-precipitated with GliZ (Table 4). Their potential relationship to GliZ and role in the response to GT or Zn treatment requires further research.

Analysis of the intracellular proteome of *A. fumigatus* Δ*gliZ*::HA-*gliZ* after induction with DOX provided an insight into the fungal response to triggering GT biosynthesis via expression of GliZ. In the presence of GT, several proteins important for both the production of, and self-protection against, intracellular GT are uniquely identified or increased in abundance. While three *gli* cluster proteins (GliG, GliN and GliM) and a novel methyltransferase MtrA, recently characterised by (de Castro et al., 2022) to be involved in the protection of *Aspergilli* against GT toxicity, are only identified with exogenous GT addition, both GliT and GtmA are found in all tested conditions and increased in abundance in response to the GT challenge. This supports previous findings which show that GT positively regulates its own biosynthesis by upregulating *gli* cluster expression (Cramer et al., 2006; Schrettl et al., 2010). Furthermore, the significantly elevated abundance of GSH synthetase (AFUA_5G06610; Table 2) in GT, compared to Zn^{2+} presence, allied to unique detection of glutathione S-transferase GliG (essential for GT biosynthesis) and an assimilatory sulfite reductase (Table 6), further consolidate an increased requirement for sulphur upon initiation of GT biosynthesis. This is in accordance with previous demonstration of

integrated sulphur metabolism in *A. fumigatus* (Sheridan et al., 2016; Traynor et al., 2019), but supplements this previous observation by implicating a requirement for an assimilatory sulfite reductase. Moreover, it underpins the proposal that sulphur metabolism is an emerging anti-fungal drug target in *A. fumigatus*, as a consequence of its potential integration into hitherto unexpected cellular systems (Amich, 2022). Indeed, if the GT/DTG couple play a role in Zn^{2+} acquisition, regulation of GliZ activity or intracellular homeostasis (Saleh et al., 2018; Seo et al., 2019; Vicentefranqueira et al., 2018), the sulphur link assumes even further importance as it may have additional functionality in facilitating zinc uptake. Interestingly, it has been recently suggested that increased availability of GSH can increase production of the ETP, chetomin, in *Chaetomium cochliodes* SD-280, further consolidating the requirement for this *S*-containing metabolite in non-ribosomal peptide biosynthesis (Zhao et al., 2022).

This work has revealed information about the connection between GT biosynthesis and zinc availability via the Zn^{2+}-dependent transcription factor GliZ. Importantly, new data about the link between sulphur metabolism (Scott et al., 2020) and regulation of GT production has been brought to light. The necessity for new strategies to control and treat *A. fumigatus* infections is highlighted by the inclusion of this pathogen as one of critical priority in the World Health Organisation's Fungal Priority Pathogen List (FPPL) (WHO, 2022); https://www.who.int/publications/i/item/9789240060241). Restriction of metal ions such as zinc and iron, as well as targeting essential sulphur metabolism may be attractive targets for antifungal research developments. Further research is needed to dissect the molecular mechanisms of GliZ, GT, and *gli* cluster activation and the importance of zinc and sulphur availability or restriction in this process.

Declaration of Competing Interest

The authors declare that they have no known competing financial interests or personal relationships that could have appeared to influence the work reported in this paper.

Acknowledgements

AMT was funded by a John and Pat Hume PhD Scholarship from Maynooth University. ÖSB was funded by an Irish Research Council Government of Ireland Post-Doctoral Fellowship (GOIPD/2014/178). LC-MS and HPLC facilities were funded by competitive awards from Science Foundation Ireland (12/RI/2346 (3)), to SD, and the Irish Higher Education Authority, respectively. qRT-PCR instrumentation was funded by Science Foundation Ireland (SFI/07/RFP/GEN/F571/ECO7). JAC was supported by the Ministerio de Ciencia e Innovación (Spain) through grant PID2019-110994RB-I00. Image station for visualization of immunoblots was funded by Science Foundation Ireland Career Development Award (13/CDA/2142). Dr Nicola Moloney is acknowledged for assistance in the early stage of this work.

Author statement

AMT and OSB carried out experimental work. SD and OB conceived and directed the work. JAC edited the manuscript and provided intellectual input. All authors wrote, reviewed and approved the final manuscript. SD is corresponding author.

References

Amich, J., Schafferer, L., Haas, H., Krappmann, S., 2013. Regulation of sulphur assimilation is essential for virulence and affects iron homeostasis of the human-pathogenic mould Aspergillus fumigatus. PLoS Pathog 9, e1003573.

Amich, J., Dümig, M., O'Keeffe, G., Binder, J., Doyle, S., Beilhack, A., Krappmann, S., 2016. Exploration of sulfur assimilation of Aspergillus fumigatus reveals biosynthesis of sulfur-containing amino acids as a virulence determinant. Infect. Immun. 84, 917–929.

Amich, J., 2022. Sulfur metabolism as a promising source of new antifungal targets. J Fungi (Basel) 8, 295.

Bacher, P., Kniemeyer, O., Teutschbein, J., Thön, M., Vödisch, M., Wartenberg, D., Scharf, D.H., Koester-Eiserfunke, N., Schütte, M., Dübel, S., Assenmacher, M., Brakhage, A.A., Scheffold, A., 2014. Identification of immunogenic antigens from Aspergillus fumigatus by direct multiparameter characterization of specific conventional and regulatory CD4+ T cells. J. Immunol. 193, 3332–3343.

Bayram, Ö.S., Dettmann, A., Karahoda, B., Moloney, N.M., Ormsby, T., McGowan, J., Cea-Sánchez, S., Miralles-Durán, A., Brancini, G.T.P., Luque, E.M., Fitzpatrick, D.A., Cánovas, D., Corrochano, L.M., Doyle, S., Selker, E.U., Seiler, S., Bayram, Ö., 2019. Control of Development, Secondary Metabolism and Light-Dependent Carotenoid Biosynthesis by the Velvet Complex of Neurospora crassa. Genetics 212, 691–710.

Bok, J.W., Chung, D., Balajee, S.A., Marr, K.A., Andes, D., Nielsen, K.F., Frisvad, J.C., Kirby, K.A., Keller, N.P., 2006. GliZ, a transcriptional regulator of gliotoxin biosynthesis, contributes to Aspergillus fumigatus virulence. Infect. Immun. 74, 6761–6768.

Cramer, R.A., Gamcsik, M.P., Brooking, R.M., Najvar, L.K., Kirkpatrick, W.R., Patterson, T.F., Balibar, C.J., Graybill, J.R., Perfect, J.R., Abraham, S.N., Steinbach, W.J., 2006. Disruption of a nonribosomal peptide synthetase in Aspergillus fumigatus eliminates gliotoxin production. Eukaryot. Cell 5, 972–980.

de Castro, P.A., Colabardini, A.C., Moraes, M., Horta, M.A.C., Knowles, S.L., Raja, H.A., Oberlies, N.H., Koyama, Y., Ogawa, M., Gomi, K., Steenwyk, J.L., Rokas, A., Gonçales, R.A., Duarte-Oliveira, C., Carvalho, A., Ries, L.N.A., Goldman, G.H., 2022. Regulation of gliotoxin biosynthesis and protection in Aspergillus species. PLoS Genet. 18, e1009965.

Dolan, S.K., Bock, T., Hering, V., Owens, R.A., Jones, G.W., Blankenfeldt, W., Doyle, S., 2017. Structural, mechanistic and functional insight into gliotoxin bis-thiomethylation in Aspergillus fumigatus. Open Biol. 7, 160292.

Elramli, N., Karahoda, B., Sarikaya-Bayram, Ö., Frawley, D., Ulas, M., Oakley, C.E., Oakley, B.R., Seiler, S., Bayram, Ö., 2019. Assembly of a heptameric STRIPAK complex is required for coordination of light-dependent multicellular fungal development with secondary metabolism in Aspergillus nidulans. PLoS Genet. 15 (3), e1008053.

Forseth, R.R., Fox, E.M., Chung, D., Howlett, B.J., Keller, N.P., Schroeder, F.C., 2011. Identification of cryptic products of the gliotoxin gene cluster using NMR-based comparative metabolomics and a model for gliotoxin biosynthesis. J. Am. Chem. Soc. 133, 9678–9681.

Frawley, D., Greco, C., Oakley, B., Alhussain, M.M., Fleming, A.B., Keller, N.P., Bayram, Ö., 2020. The tetrameric pheromone module SteC-MkkB-MpkB-SteD regulates asexual sporulation, sclerotia formation and aflatoxin production in Aspergillus flavus. Cell. Microbiol. 22, e13192.

Gomez-Lopez, A., Rueda, C., Pando Pozo, R., Sanchez Gonzalez, L.M., 2022. Dynamics of gliotoxin and bis(methylthio)gliotoxin production during the course of Aspergillus fumigatus infection. Med 60 (4), myac025.

Health, World, n.d. Organisation's Fungal Priority Pathogen List (FPPL). https://www.who.int/publications/i/item/9789240060241.

Helmschrott, C., Sasse, A., Samantaray, S., Krappmann, S., Wagener, J., 2013. Upgrading fungal gene expression on demand: improved systems for doxycycline-dependent silencing in Aspergillus fumigatus. Appl. Environ. Microbiol. 79, 1751–1754.

Huang, Z.L., Ye, W., Zhu, M.Z., Kong, Y.L., Li, S.N., Liu, S., Zhang, W.M., 2019. Interaction of a novel Zn_2Cys_6 transcription factor DcGliZ with promoters in the gliotoxin biosynthetic gene cluster of the deep-sea-derived fungus dichotomomyces cejpii. Biomolecules 10, 56.

König, S., Pace, S., Pein, H., Heinekamp, T., Kramer, J., Romp, E., Straßburger, M., Troisi, F., Proschak, A., Dworschak, J., Scherlach, K., Rossi, A., Sautebin, L., Haeggström, J.Z., Hertweck, C., Brakhage, A.A., Gerstmeier, J., Proschak, E., Werz, O., 2019. Gliotoxin from Aspergillus fumigatus Abrogates Leukotriene B(4) Formation through Inhibition of Leukotriene A(4) Hydrolase. Cell Chem. Biol. 26, 524–534.e525.

Liu, H., Xu, W., Solis, N.V., Woolford, C., Mitchell, A.P., Filler, S.G., 2018. Functional convergence of gliP and aspf1 in Aspergillus fumigatus pathogenicity. Virulence 9, 1062–1073.

Liu, H., Xu, W., Bruno, V.M., Phan, Q.T., Solis, N.V., Woolford, C.A., Ehrlich, R.L., Shetty, A.C., McCraken, C., Lin, J., Bromley, M.J., Mitchell, A.P., Filler, S.G., 2021. Determining Aspergillus fumigatus transcription factor expression and function during invasion of the mammalian lung. PLoS Pathog. 17, e1009235.

Marion, A., Groll, M., Scharf, D.H., Scherlach, K., Glaser, M., Sievers, H., Schuster, M., Hertweck, C., Brakhage, A.A., Antes, I., Huber, E.M., 2017. Gliotoxin Biosynthesis: Structure, Mechanism, and Metal Promiscuity of Carboxypeptidase GliJ. ACS Chem. Biol. 12, 1874–1882.

Mulvihill, E.D., Moloney, N.M., Owens, R.A., Dolan, S.K., Russell, L., Doyle, S., 2017. Functional investigation of iron-responsive microsomal proteins, including MirC, in Aspergillus fumigatus. Front. Microbiol. 8, 418.

Nielsen, M.L., Albertsen, L., Lettier, G., Nielsen, J.B., Mortensen, U.H., 2006. Efficient PCR-based gene targeting with a recyclable marker for Aspergillus nidulans. Fungal Genet. Biol. 43, 54–64.

O'Hanlon, K.A., Gallagher, L., Schrettl, M., Jöchl, C., Kavanagh, K., Larsen, T.O., Doyle, S., 2012. Nonribosomal peptide synthetase genes pesL and pes1 Are essential for fumigaclavine C production in Aspergillus fumigatus. Appl. Environ. Microbiol. 78, 3166–3176.

O'Keeffe, G., Hammel, S., Owens, R.A., Keane, T.M., Fitzpatrick, D.A., Jones, G.W., Doyle, S., 2014. RNA-seq reveals the pan-transcriptomic impact of attenuating the gliotoxin self-protection mechanism in Aspergillus fumigatus. BMC Genomics 15 (1), 894.

Owens, R.A., O'Keeffe, G., Smith, E.B., Dolan, S.K., Hammel, S., Sheridan, K.J., Fitzpatrick, D.A., Keane, T.M., Jones, G.W., Doyle, S., 2015. Interplay between

Gliotoxin Resistance, Secretion, and the Methyl/Methionine Cycle in Aspergillus fumigatus. Eukaryot. Cell 14, 941–957.
Raudvere, U., Kolberg, L., Kuzmin, I., Arak, T., Adler, P., Peterson, H., Vilo, J., 2019. g: Profiler: a web server for functional enrichment analysis and conversions of gene lists (2019 update). Nucleic Acids Res. 47, W191–W198.
Saleh, A.A., Jones, G.W., Tinley, F.C., Delaney, S.F., Alabbadi, S.H., Fenlon, K., Doyle, S., Owens, R.A., 2018. Systems impact of zinc chelation by the epipolythiodioxopiperazine dithiol gliotoxin in Aspergillus fumigatus: a new direction in natural product functionality. Metallomics 10, 854–866.
Scharf, D.H., Remme, N., Heinekamp, T., Hortschansky, P., Brakhage, A.A., Hertweck, C., 2010. Transannular disulfide formation in gliotoxin biosynthesis and its role in self-resistance of the human pathogen Aspergillus fumigatus. J Am Chem Soc 132, 10136–10141.
Scharf, D.H., Habel, A., Heinekamp, T., Brakhage, A.A., Hertweck, C., 2014. Opposed effects of enzymatic gliotoxin N- and S-methylations. J. Am. Chem. Soc. 136, 11674–11679.
Schindelin, J., Arganda-Carreras, I., Frise, E., Kaynig, V., Longair, M., Pietzsch, T., Preibisch, S., Rueden, C., Saalfeld, S., Schmid, B., Tinevez, J.Y., White, D.J., Hartenstein, V., Eliceiri, K., Tomancak, P., Cardona, A., 2012. Fiji: an open-source platform for biological-image analysis. Nat. Methods 9, 676–682.
Schrettl, M., Carberry, S., Kavanagh, K., Haas, H., Jones, G.W., O'Brien, J., Nolan, A., Stephens, J., Fenelon, O., Doyle, S., 2010. Self-protection against gliotoxin-a component of the gliotoxin biosynthetic cluster, gliT, completely protects Aspergillus fumigatus against exogenous gliotoxin. PLoS Pathogens 6, e1000952.
Scott, J., Sueiro-Olivares, M., Thornton, B.P., Owens, R.A., Muhamadali, H., Fortune-Grant, R., Thomson, D., Thomas, R., Hollywood, K., Doyle, S., Goodacre, R., Tabernero, L., Bignell, E., Amich, J., 2020. Targeting methionine synthase in a fungal pathogen causes a metabolic imbalance that impacts cell energetics, growth, and virulence. mBio 11 (5), e01985-20.
Schmaler-Ripcke, J., Sugareva, V., Gebhardt, P., Winkler, R., Kniemeyer, O., Heinekamp, T., Brakhage, A.A., 2009. Production of pyomelanin, a second type of melanin, via the tyrosine degradation pathway in Aspergillus fumigatus. Appl Environ Microbiol 75, 493–503.
Seo, H., Kang, S., Park, Y.S., Yun, C.W., 2019. The Role of Zinc in Gliotoxin Biosynthesis of Aspergillus fumigatus. Int. J. Mol. Sci. 20 (24), 6192.
Sheridan, K.J., Lechner, B.E., Keeffe, G.O., Keller, M.A., Werner, E.R., Lindner, H., Jones, G.W., Haas, H., Doyle, S., 2016. Ergothioneine biosynthesis and functionality in the opportunistic fungal pathogen, Aspergillus fumigatus. Scientific Reports 6, 35306.
Shevchenko, A., Tomas, H., Havlis, J., Olsen, J.V., Mann, M., 2006. In-gel digestion for mass spectrometric characterization of proteins and proteomes. Nat. Protoc. 1, 2856–2860.
Singh, B., Sharma, G.L., Oellerich, M., Kumar, R., Singh, S., Bhadoria, D.P., Katyal, A., Reichard, U., Asif, A.R., 2010. Novel cytosolic allergens of Aspergillus fumigatus identified from germinating conidia. J Proteome Res 9, 5530–5541.
Thon, M., Al Abdallah, Q., Hortschansky, P., Scharf, D.H., Eisendle, M., Haas, H., Brakhage, A.A., 2010. The CCAAT-binding complex coordinates the oxidative stress response in eukaryotes. Nucleic Acids Res. 38, 1098–1113.
Traynor, A.M., Sheridan, K.J., Jones, G.W., Calera, J.A., Doyle, S., 2019. Involvement of Sulfur in the Biosynthesis of Essential Metabolites in Pathogenic Fungi of Animals, Particularly Aspergillus spp.: Molecular and Therapeutic Implications. Front. Microbiol. 10, 2859.
Traynor, A.M., Owens, R.A., Coughlin, C.M., Holton, M.C., Jones, G.W., Calera, J.A., Doyle, S., 2021. At the metal-metabolite interface in Aspergillus fumigatus: towards untangling the intersecting roles of zinc and gliotoxin. Microbiology (Reading) 167 (11), 001106.
Vicentefranqueira, R., Amich, J., Marin, L., Sanchez, C.I., Leal, F., Calera, J.A., 2018. The transcription factor ZafA regulates the homeostatic and adaptive response to zinc starvation in Aspergillus fumigatus. Genes (Basel) 9 (7), 318.
Vicentefranqueira, R., Leal, F., Marín, L., Sánchez, C.I., Calera, J.A., 2019. The interplay between zinc and iron homeostasis in Aspergillus fumigatus under zinc-replete conditions relies on the iron-mediated regulation of alternative transcription units of *zafA* and the basal amount of the ZafA zinc-responsiveness transcription factor. Environ. Microbiol. 21, 2787–2808.
Ye, W., Zhang, W., Liu, T., Huang, Z., Zhu, M., Chen, Y., Li, H., Li, S., 2018. De novo transcriptome sequencing of the deep-sea-derived fungus dichotomomyces cejpii and analysis of Gliotoxin biosynthesis genes. Int. J. Mol. Sci. 19 (7), 1910.
Ye, W., Li, S., Liu, S., Kong, Y., Zhang, W., Liu, T., 2021a. Characterization of novel gliotoxin biosynthesis-related genes from deep-sea-derived fungus Geosmithia pallida FS140. Biochimie 191, 1–10.
Ye, W., Liu, T., Zhang, W., 2021b. The Toxic Mechanism of Gliotoxins and Biosynthetic Strategies for Toxicity Prevention. Int. J. Mol. Sci. 22.
Yu, J.H., Hamari, Z., Han, K.H., Seo, J.A., Reyes-Domínguez, Y., Scazzocchio, C., 2004. Double-joint PCR: a PCR-based molecular tool for gene manipulations in filamentous fungi. Fungal Genet. Biol. 41, 973–981.
Zhao, P., Liu, H., Wu, Q., Meng, Q., Qu, K., Yin, X., Wang, M., Zhao, X., Qi, J., Meng, Y., Xia, X., Zhang, L., 2022. Investigation of chetomin as a lead compound and its biosynthetic pathway. Appl. Microbiol. Biotechnol. 106, 3093–3102.